Ionics (2020) 26:875–894
https://doi.org/10.1007/s11581-019-03253-5

ORIGINAL PAPER

High selective heterogeneous cation exchange membrane modified by L-cysteine with enhanced electrochemical performance

E. Jashni[1] · S. M. Hosseini[1]

Received: 5 July 2019 / Accepted: 3 September 2019 / Published online: 13 September 2019

Abstract
This research focuses on the formation of ionic clusters and the transport properties of metal ions through electrodialysis heterogeneous cation exchange membrane modified by L-cysteine as a polar additive. The molecular electrostatic potential of L-Cyst and resin particle showed appropriate reactive sites for electrophilic and nucleophilic attacks. Furthermore, the calculated interaction energy confirmed the presence of strong interactions between the L-Cyst molecule and the resin particle. Elemental mapping, scanning electron microscopy (SEM), and scanning optical microscopy (SOM) images of the blended membranes represented a relatively uniform surface and particle distribution. Membrane water uptake and surface hydrophilicity were enhanced in the presence of L-Cyst. The blended membranes demonstrated high selectivity (> 99%), lower electrical resistance (< 5–6 Ω cm^2), and better ionic permeability compared to the bare membrane. The blended membranes (HCEM–2.0 wt% L-Cyst) showed higher dialytic rate, lower energy consumption, and current efficiency in Pb^{2+} ion removal from water compared to the bare sample.

Keywords Cation exchange membranes · Ionic clusters · L-Cysteine · Intensified electrochemical property · Lead ion removal

Introduction

Inadequate access to freshwater is among the highlighted issues facing the world today, which needs multidisciplinary and global solutions. Nowadays, we are facing with the expansion of the industrial and agriculture activities together with enhancing living standards which are expected to worsen the water crisis. The critical imbalance between freshwater usage and its available supply has led to an increasing demand for converting nonpotable sources to water-appropriate human use. In the meantime, desalination, a process that takes pure water away from saline water, will likely become a vital source of freshwater for a thirsty world. In spite of seawater which is abundant (constitutes over 97% of water resources on the globe), desalination to date merely occupies a small fraction of the freshwater preparation [1–3]. Electrodialysis (ED), the most widely adopted commercial desalination technology, has a staggering potential of producing potable water from sea water. This technology employs electrically charged ion exchange membranes (IEMs) that transport anions through anion exchange membranes (AEMs) and cations through cation exchange membranes (CEMs). These membranes are famed thanks to their unique features and are utilized in several industries for numerous electrochemical applications based on separation techniques. IEMs are the heart of an ED process and affect both efficiency and practical application value for it [4–7]. Although the advancement in exploring IEMs has evolved rapidly, there are still few challenges, which need to be addressed. To date, most studies dealing with IEMs have been focused on expanding various fabrication methods, exploring promising materials, and developing a wide variety of applications. Nevertheless, research on the IEMs' performance details is not fully mature, and there are several stages in which improvements are still necessary. Understanding well the underlying transportation mechanism and performance details not only provides fundamental knowledge for the progress of IEMs but also opens up the opportunity to addressing IEMs' challenges. In other words, if complex phenomena occurring into the IEMs were well studied and understood, it would be possible to find a right solution in order to solve their challenges. Therefore, much endeavor is needed to unite

✉ S. M. Hosseini
s-hosseini@araku.ac.ir

[1] Department of Chemical Engineering, Faculty of Engineering, Arak University, Arak 3815688349, Iran

theoretical, experimental, and simulation data for a more exhaustive understanding of IEMs phenomena. In the scope of the present work, we will deeply discuss IEMs performance details and their transportation behavior. The main emphasis will be on the effect of interaction between IEMs' constituent particles on the formation of ionic clusters and transport properties of metal ions, which have not been checked in-depth in most cases. Particle dispersion plays a considerable role in optimizing the electrochemical characteristics of IEMs. Although it is essential to homogeneously distribute the particles in the polymer matrix to attain the optimum benefit from the advantages of both phases, it is difficult to attain fine dispersion and compact morphology in practice because of the discrepancies in component chemistry and dimensional structures. The severe aggregation of additives and their weak compatibility with the polymer matrix are the key limitations hampering to the successful incorporation of additives to the polymer film. These two phenomena bring about the formation of nonselective voids at the interface of the polymer and additive, which is the Achilles heel of IEMs. Given that there is a direct link between polarity of additives (presence of polar parts in their chemical structures), interaction between additives and particles, and their distribution in the membrane matrix, it seems that polar additives can be promising candidates for overcoming the discussed challenges. What's more, these polar materials have tremendous potential applications in adsorption and antifouling properties which have attracted significant research interest in recent years [8–12]. Based on the mentioned preface, we selected L-Cyst as a polar additive to achieve targeted properties. It is a well-established fact that IEMs' morphology and electrochemical properties have a drastic affiliation to the interactions between their constituent components. Therefore, it seems that the proposed additive owing to its three functional groups (thiol (SH), carboxyl (–COOH), and amine ($–NH_2$)), which can act as proper reactive sites for interaction with resin particles, is a good candidate for this probe. Amino acids' basic unit has $–NH_2$ and –COOH functional groups that can act as linkers for their interaction with other materials. L-Cyst is the only natural thiol-containing amino acid with excellent water solubility. It possesses antibacterial behavior and metal-binding properties due to its three functional groups (–SH, $–NH_2$, –COOH) [13, 14].

To study the transport behavior of metal ions in prepared membranes, Na^+ as a common monovalent ion and Pb^{2+} as a divalent heavy metal were chosen. Heavy metals have been a challenge for the water treatment industry for decades because they cannot be degraded by natural biological mechanisms. Pb^{2+} is one of the most harmful heavy metals. The environmental consequences of Pb^{2+} ion accumulation have been linked to detrimental health impacts in humans. Hence, the transport behavior and removal of Pb^{2+} ions were studied in this work [15–18].

Materials and methods

Materials

The materials used are shown in Table 1.

Methods

IEM fabrication

The cation exchange membranes were provided by the solution casting technique. In order to provide the casting solution, a polymer binder (PVC) was dissolved into solvent (THF) in a glass reactor (1:20) (w/v) and stirred for 4 h. Subsequently, a certain amount of ground resin particles was dispersed in the solution by a mechanical stirrer (Model: Velp Sientifica Multi 6 stirrer). The L-Cyst particles were also added as additive in the polymeric solution (the ratios of L-Cyst (additive/total solid) in samples 1–6 were as follows: 0.0/100 (w/w), 0.5/100 (w/w), 1.0/100 (w/w), 2.0/100 (w/w), 4.0/100 (w/w), and 8.0/100 (w/w), respectively). The casting solutions were then sonicated for 1 h using an ultrasonic instrument (Parsonic11 S model, S/N PN-88159, Iran). Application of ultrasound radiation allows achieving a better homogeneity in the matrix of fabricated membranes. It promotes the adaptability between polymer and particles by reducing sedimentation and aggregation. The resulting solution was then casted as a thin film on

Table 1 Materials used in this research

Material	Application	Feature	Company
Polyvinylchloride (PVC)	Polymer	Grade S-7054, density 490 g/l, viscosity number 105 cm^3/g	BIPC Company, Iran
Tetrahydrofuran (THF)	Solvent	Mw 72.11, density 0.89 g/cm^3	Merck, Germany
Cation exchange resin	Resin	Ion exchanger Amberlyst[15], strongly acidic cation exchanger, H^+ form with more than 1.7 meq/l, density 0.6 g/cm^3	Merck, Germany
L-Cysteine	Additive	Lab grade	Sigma-Aldrich, USA
NaCl	–	Lab grade	Merck, Germany
$Pb(NO_3)_2$	–	Lab grade	Merck, Germany

a clean and dry glass plate at ambient temperature. After evaporation, the membranes were soaked in distilled water. Finally, the nanocomposite membranes were kept in 0.1 M NaCl solution [19–22]. The steps of membrane preparation and the composition of the casting solution are given in Tables 2 and 3, respectively.

IEM test cell

In this research, a test cell has been applied in order to specify the membranes' electrochemical properties. A visual representation of this cell which is made of different parts is shown in Fig. 1.

Characterizations

Fourier transform infrared spectra

To provide information about the chemical structure of the prepared membranes, dried membrane samples were analyzed by a single beam Fourier transform-infrared (FT-IR) spectrometer (Galaxy series 5000) in the range from 4000 to 200 cm^{-1}.

Morphological characterization

In this probe, the morphology of resultant membranes was tested by EDX spectrum, elemental mapping, scanning electron microscopy (SEM), and scanning optical microscopy (SOM) techniques. To investigate the surface morphology of the fabricated membranes and the effect of roughness on the separation efficiency, 3D surface images were prepared using optical microscopy and SPIP software (version 6.4) in the area of 7.5 μm × 10 μm. The interaction between membrane–solutes and membrane–solvents depends largely on the affinity of the membrane materials to liquids. The surface hydrophilicity of the fabricated membranes was characterized by the contact angle ( ) measurements. These angles were determined using the water drop method on dry membrane.

Water uptake

The water uptake (WU) of an IEM was evaluated in terms of the ratio of the amounts of adsorbed water to dry weight of the corresponding membrane samples. Prior to analysis, the membranes were soaked in DI water for 48 h. Then the soaked samples were weighed immediately after using tissue paper to wipe off the water on the membrane surface (wet weight). Afterwards, the wet membranes were dried at 70 °C until obtaining a constant weight and then weighed again (dry weight). WU was specified using Eq. (1) [23–25]:

$$\mathrm{WU}\ \% = \left(\frac{m_{\mathrm{wet}} - m_{\mathrm{dry}}}{m_{\mathrm{dry}}}\right) \times 100 \tag{1}$$

Electrochemical behavior

The membrane potential, transport number, and permselectivity of investigated membranes were determined at room temperature. The samples were first maintained in 0.1 M NaCl solution for at least 24 h and then placed in the IEM test cell. The concentration of NaCl solutions was 0.1 M in anodic section and 0.01 M in cathodic section. The diffusion potential across the membrane was measured with two calomel reference electrodes and a voltmeter. The membrane potential (E_{Measure}) is expressed using the Nernst equation as follows:

$$E = \left(2t_{\mathrm{i}}^{\mathrm{m}} - 1\right)\left(\frac{RT}{nF}\right)\ln\left(\frac{a_1}{a_2}\right) \tag{2}$$

where $t_{\mathrm{i}}^{\mathrm{m}}$ is the transport number of counter ions in the membrane phase, R is the universal gas constant, T is the temperature (K), n is electrovalence of counter ion, and a_1 and a_2 are the solution electrolyte activities in contact with surfaces determined by the Debye–Hückel limiting law.

The ionic permselectivity of membranes (Ps) is also quantitatively expressed based on the migration of counter ions through the IEMs:

$$\mathrm{Ps} = \frac{t_{\mathrm{i}}^{\mathrm{m}} - t_0}{1 - t_0} \tag{3}$$

Table 2 Summary of the membrane preparation procedure

IEM preparation	
Step 1	Resin particles pulverizing (− 300 + 400 mesh)
Step 2	Polymer (PVC) dissolving into tetrahydrofuran (for 4 h)
Step 3	Resin particles and additive (L-cysteine) dispersing in polymeric solution
Step 4	Sonication of polymeric solution (for 1 h)
Step 5	Mixing of polymeric solution (for another 30 min)
Step 6	Casting (at ambient temperature)
Step 7	Film drying (at ambient temperature for 30 min) and immersing in water

Table 3 Composition of casting solution used in the preparation of home-made membranes

Membrane[a] (sample)	L-Cysteine (L-cysteine:(PVC + resin)), (w/w)
Sample 1	0.0:100
Sample 2	0.5:100
Sample 3	1.0:100
Sample 4	2.0:100
Sample 5	4.0:100
Sample 6	8.0:100

[a] (Solvent (THF:PVC) (v/w), (20:1); resin particles (resin:PVC) (w/w), (1:1))

where t_0 is the transport number of counter ions in solution [23–25].

NaCl solution was employed to measure the ionic permeability and flux. A direct current electrical potential (DC power supply, Model: PS-302D) with an optimum constant voltage (10 V) was applied by platinum electrode. During the process, the migration of cations occurs through the membrane to the cathodic zone. The Na^+ permeability and flux can be measured by considering pH changes in cathodic region as described elsewhere [23–25].

The electrical resistance of equilibrated IEMs was measured in NaCl solution with 0.5 M concentration. Measurements were carried out by an alternating current bridge with 1500 Hz frequency (Audio single generator, Electronic Afzar Azma Co. P.J.S). Then, membrane electrical resistance (MER) was calculated according to:

$$R_m = R_{m+s} - R_s \tag{4}$$

where R_m is the transverse electric resistance of the membrane (in Ω), R_{m+s} is the resistance of the membrane and the reference solution measured together (in Ω), and R_s the resistance of the reference solution (in Ω).

The areal resistance was expressed as follows:

$$r = (R_m A) \tag{5}$$

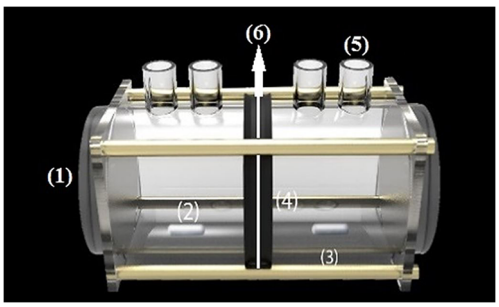

Fig. 1 Schematic diagram of the test cell used in this study: (1) Pt electrode, (2) magnetic bar, (3) stirrer, (4) rubber ring, (5) orifice, (6) membrane

where r is the areal resistance and A is the surface area (cm^2) of the membrane.

Moreover, the ionic conductivity (IC) of the prepared membranes (S/cm) was calculated based on the electrical resistance measurement, following the equation [23–25]:

$$\mathrm{IC} = \frac{L}{r} \tag{6}$$

where L is the membrane thickness (cm).

To examine the performance of the prepared membranes in Pb^{2+} ion separation from water, electrodialysis experiments were carried out in a laboratory-scale unit containing a lab-made cation exchange membrane and a commercial anion exchange membrane at constant applied (15 V). A commercial heterogeneous anion exchange membrane (RALEX AMH-PES), made by MEGA a.s., Czech Republic, was utilized in this probe. An aqueous solution containing 20 ppm $Pb(NO_3)_2$ was used as feed. The treated compartment becomes dilute as the cations and anions pass through the membrane. The treated solution was collected after 15, 30, 45, 60, and 75 min and then analyzed by atomic adsorption spectroscopy.

The current efficiency (CE) was calculated using the following equation [23–25]:

$$\mathrm{CE} = \frac{F \times Z_i \times \Delta n}{\int_{t=0}^{t=t} I\,\mathrm{d}t} \tag{7}$$

And for the energy consumption (E) [23–25]:

$$E = \frac{\int_{t=0}^{t=t} I \times \mathrm{d}t \times V}{\Delta n} \tag{8}$$

where Z_i is the valance of ion, Δn is the transport number of moles, V is the voltage, F is the Faraday constant, and I is the current intensity.

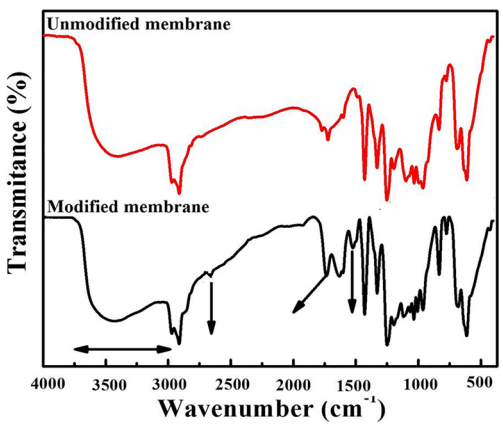

Fig. 2 FT-IR spectrum analysis of lab-made membranes: unmodified membrane and modified membrane containing L-cysteine

Results and discussion

FT-IR spectra

Figure 2 shows the FT-IR spectra of the unmodified membrane and a modified membrane containing L-Cyst. The curve of the modified membrane containing L-Cyst shows new bands which are not visible for the unmodified membrane. The characteristic band at 1520 cm^{-1} corresponds to a N–H band, and a very broad band of NH_3^+ stretching is observed for 3000–3600 cm^{-1}. The weak peak at around 2600 cm^{-1}

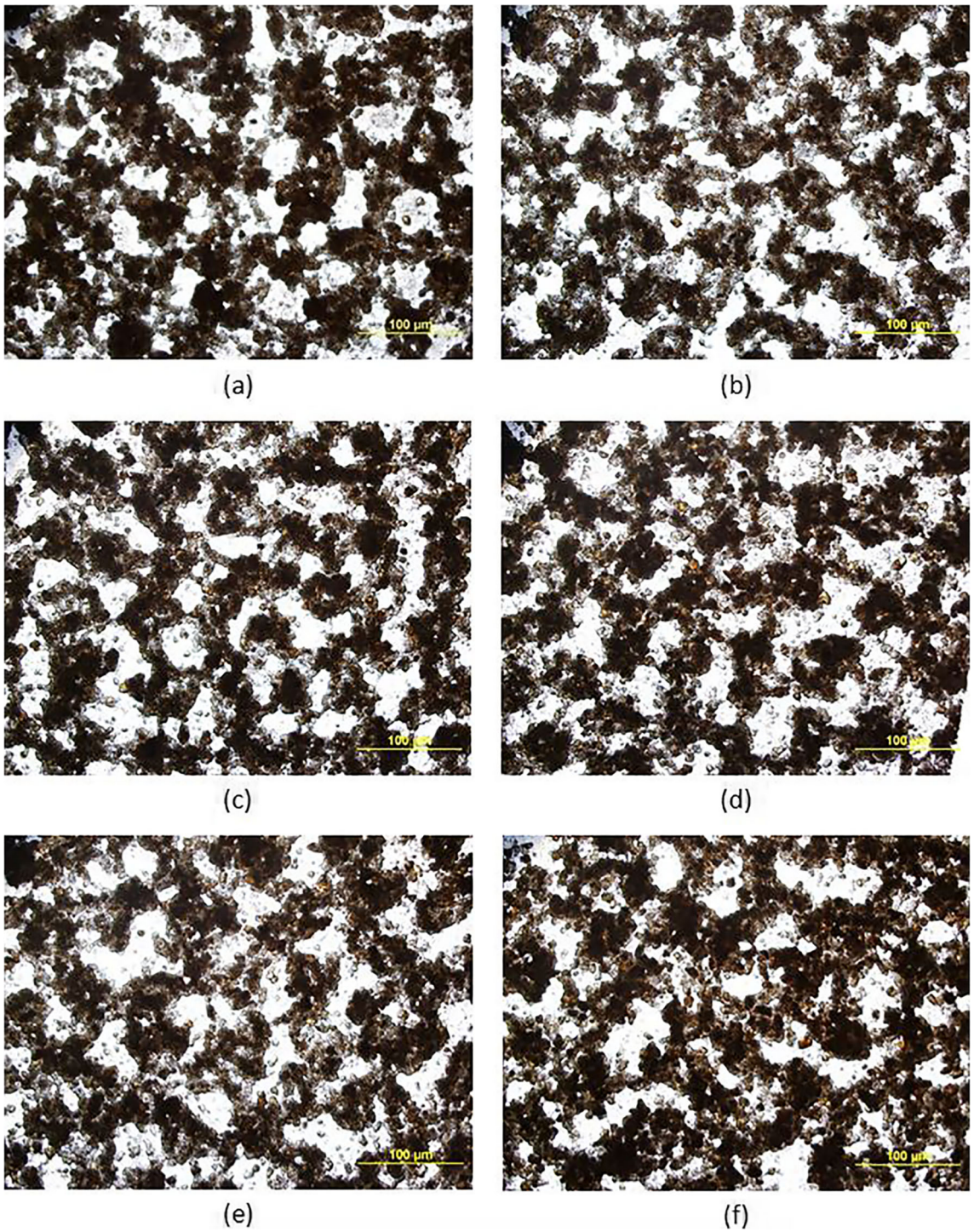

Fig. 3 The SOM images (×4 magnifications) of prepared membranes with various ratios of L-cysteine content: **a** 0.0 wt%, **b** 0.5 wt%, **c** 1.0 wt%, **d** 2.0 wt%, **e** 4.0 wt%, **f** 8.0 wt%

represents the S–H group of L-Cyst. The spectrum of the modified membrane also displays a band at 1730 cm^{-1} originating from the C=O of L-Cyst [26]. Furthermore, no chemical reaction occurs during membrane fabrication.

Surface characterization of the membranes

The surface properties of the IEMs have a remarkable effect on their electrochemical properties. For this reason, we characterized the surface properties of the newly lab-made

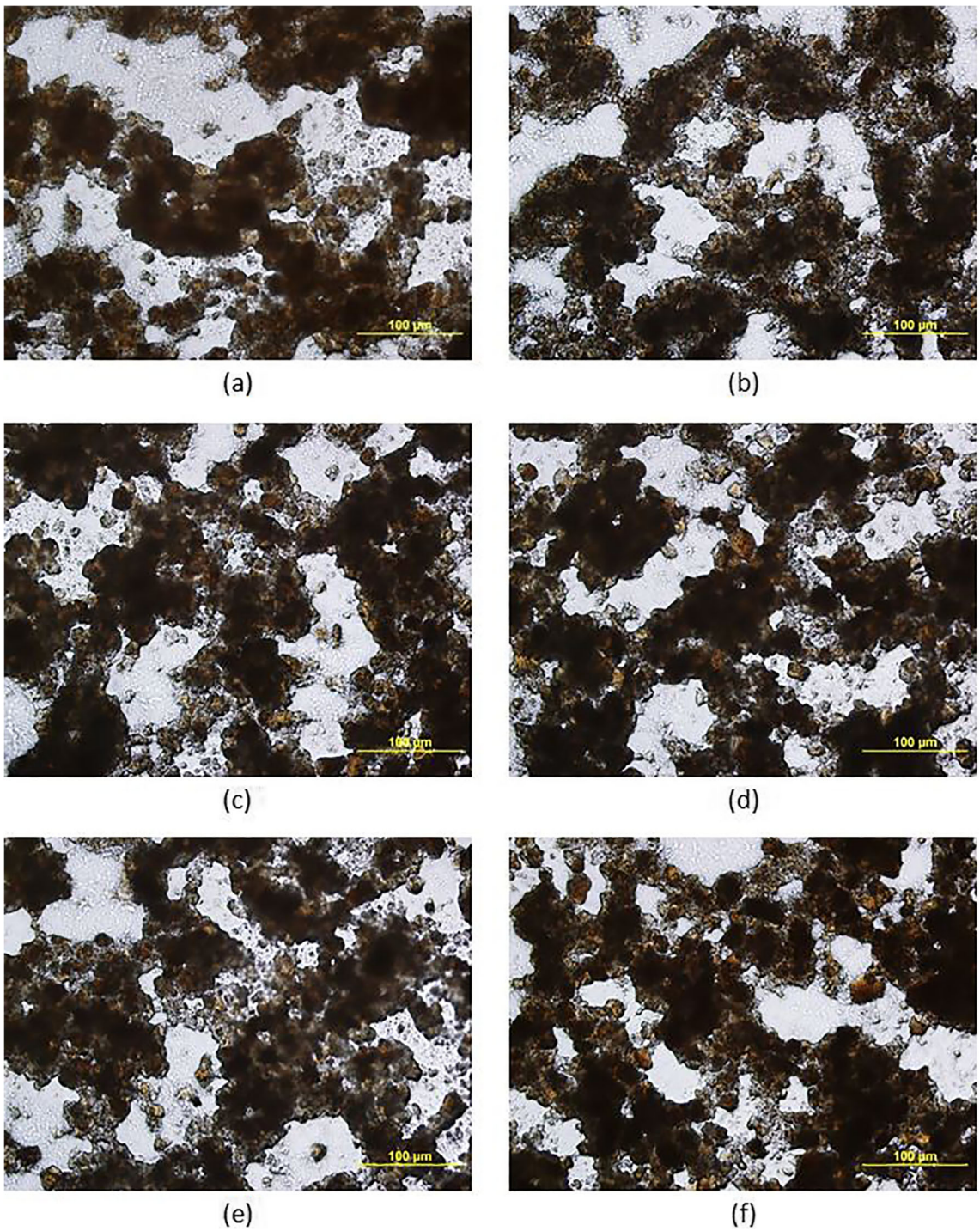

Fig. 4 The SOM images (×10 magnifications) of prepared membranes with various ratios of L-cysteine content: **a** 0.0 wt%, **b** 0.5 wt%, **c** 1.0 wt%, **d** 2.0 wt%, **e** 4.0 wt%, **f** 8.0 wt%

membranes from surface morphology, surface hydrophilicity, and surface roughness point of view.

Membrane morphology is characterized by the interfacial morphology (interfacial voids, pore blocked region, and rigidity of polymer chain layers) and particle dispersion (in an ordered pattern, randomly, and in the form of agglomeration). The interfacial morphology can dictate the whole electrochemical and mechanical features, whereas particle dispersion controls the optimization of the component characteristics and their synergism in manipulating the relation among membrane water uptake, conductivity, and membrane permeability [8]. SOM (Figs. 3 and 4) and SEM (Figs. 5 and 6) images demonstrate the uniform distribution of particles in fabricated membranes. Further, elemental mapping of N (see

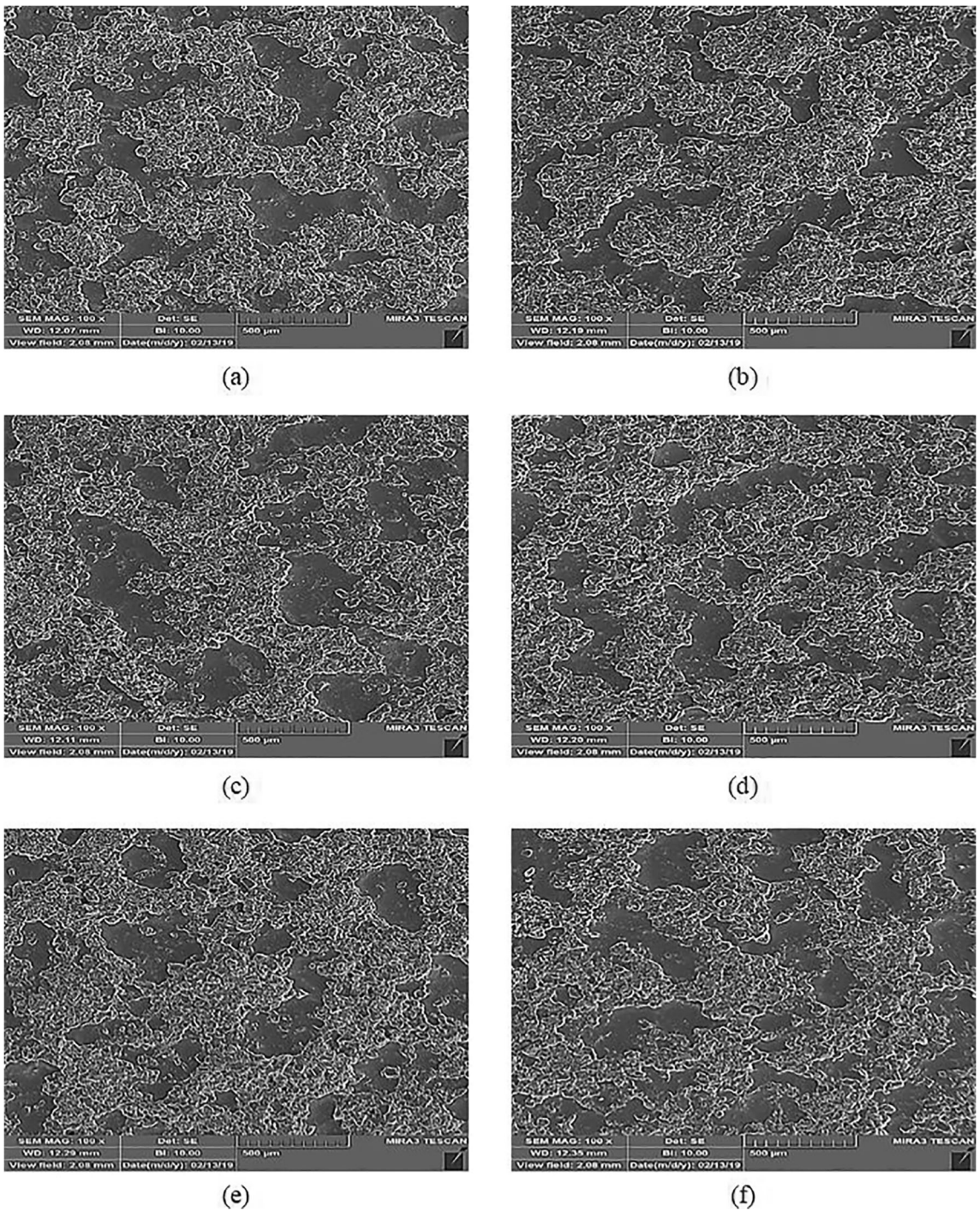

Fig. 5 The SEM images (×100 magnifications) of prepared membranes with various ratios of L-cysteine content: **a** 0.0 wt%, **b** 0.5 wt%, **c** 1.0 wt%, **d** 2.0 wt%, **e** 4.0 wt%, **f** 8.0 wt%

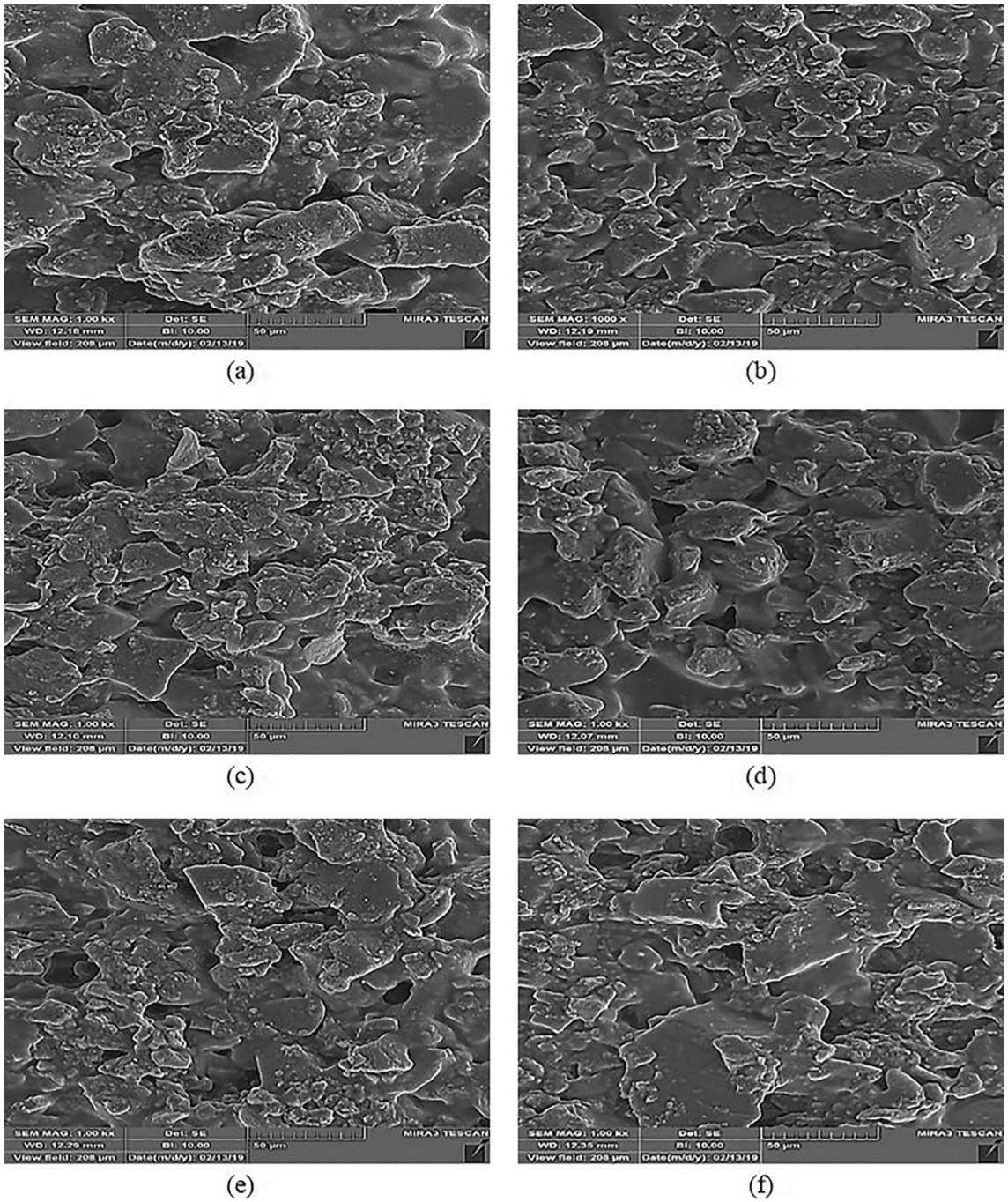

Fig. 6 The SEM images (×1000 magnifications) of prepared membranes with various ratios of L-cysteine content: **a** 0.0 wt%, **b** 0.5 wt%, **c** 1.0 wt%, **d** 2.0 wt%, **e** 4.0 wt%, **f** 8.0 wt%

Fig. 7), which is the characteristic element of L-Cyst, confirms the uniform distribution of the additive in the membrane matrix. It seems that interactions of resin particles and L-Cyst molecules led to better distribution of L-Cyst/resin particles in the membrane matrix. Figure 8 a and b show the molecular electrostatic potential (MEP) of resin particle and L-Cyst molecule, respectively (negative and positive electrostatic potential regions in MEP plots are represented by the red and blue colors, respectively). Keeping in view the MEP plots, we conclude that both particles have appropriate reactive sites for electrophilic and nucleophilic attacks. These reactive sites in resin particles and L-Cyst molecules lead to forming several interactions between them. A schematic representation of these interactions (SH … π, NH … π, OH … π, and CH … π interactions and also OH … N, OH … O, OH … S, SH … O, NH … O, CH … O, CH … N and CH … S hydrogen bonding) is demonstrated in Fig. 9. To provide conclusive evidence for the possibility of these interactions, we calculated

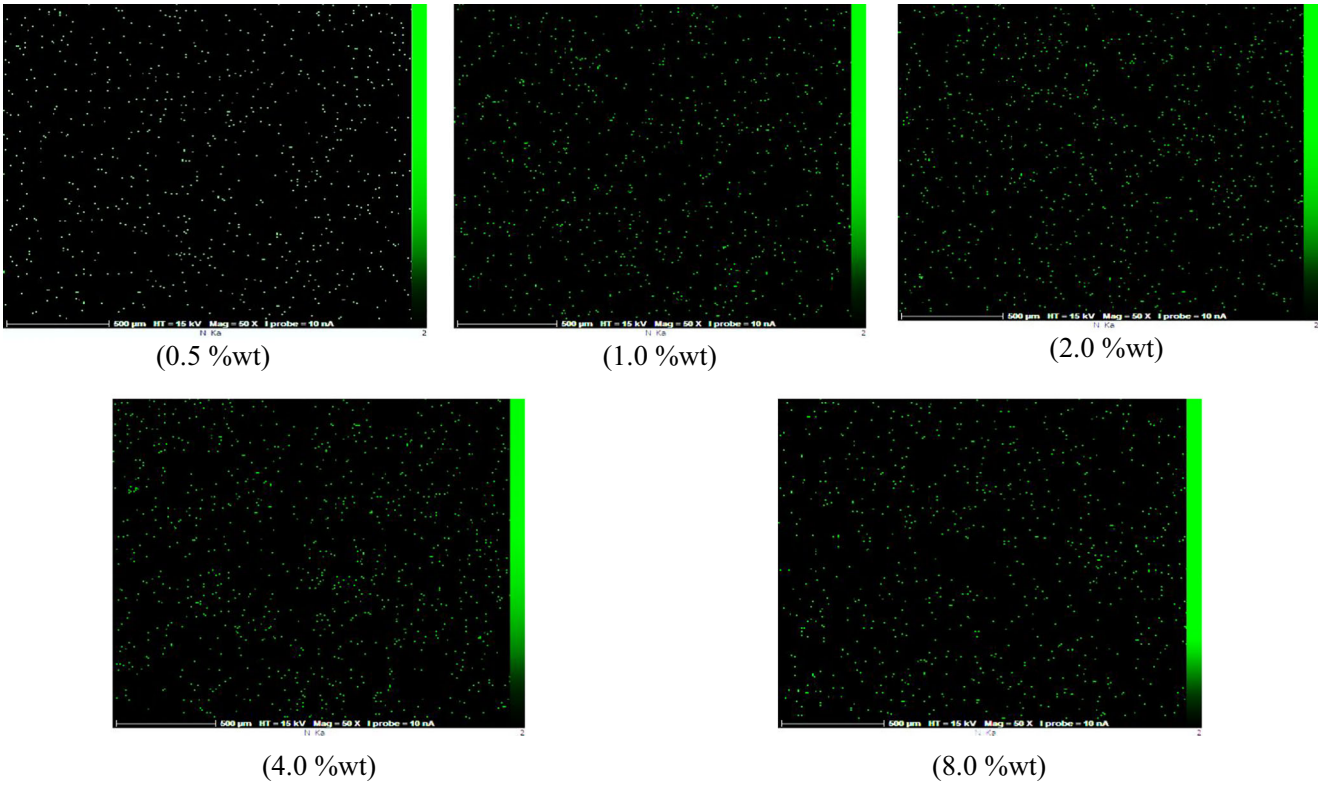

Fig. 7 EDX mapping of N element of modified membranes with various ratios of L-cysteine content: 0.5 wt%, 1.0 wt%, 2.0 wt%, 4.0 wt%, 8.0 wt%

the interaction energy between L-Cyst molecule and resin particle through their most nucleophilic and electrophilic centers (state I—NH_2 of L-Cyst as a nucleophilic center and OH of resin as an electrophilic center, state II—C=O of L-Cyst as a nucleophilic center and OH of resin as an electrophilic center, and state III—OH of L-Cyst as an electrophilic center and S=O of resin as a nucleophilic center). The results indicated that the values of energies for these states were − 27.6, − 19, and − 11 kcal/mol, respectively (All structures were optimized by cam-B3LYP method and 6-31++g (d, p) basis set. These calculations were performed using Gaussian 09 package), which confirms the presence of strong interactions between L-Cyst molecules and resin particles [14, 27]. Also, these values show that the interaction energy is the highest in magnitude when interaction occurred through state I. This can be explained by considering the fact that NH_2 is the most nucleophilic center in L-Cyst and is more prone toward bonded interactions with the electrophilic center of the resin particle. Strong interactions between L-Cyst molecules and resin particles lead to proper hydrophobic–hydrophilic architecture for resultant membranes. Furthermore, the existence of the mentioned interactions is corroborated by the SEM and elemental mapping results, which demonstrate the particles (resin particles/L-Cyst molecules), were uniform with no apparent aggregation (see Fig. 10). Generally, interactions between constituent components of IEMs are a key factor determining superior regions

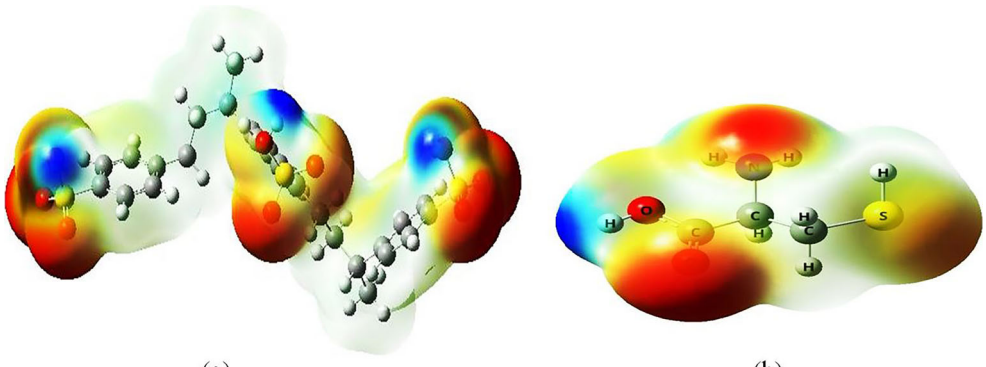

Fig. 8 Molecular electrostatic potential (MEP) of **a** resin particle and **b** L-Cyst molecule

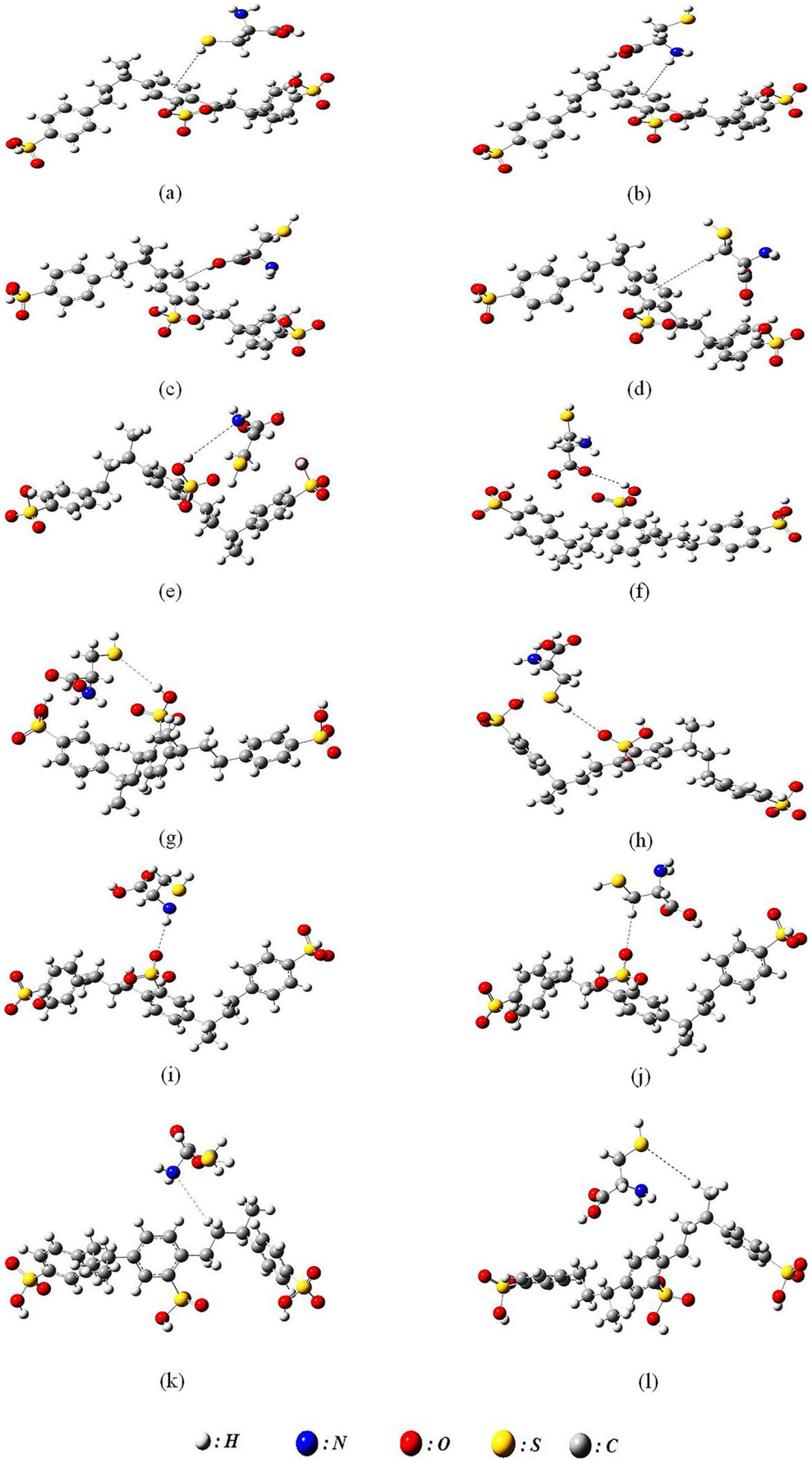
(a)
(b)
(c)
(d)
(e)
(f)
(g)
(h)
(i)
(j)
(k)
(l)
: H
: N
: O
: S
: C

◀ **Fig. 9** Schematic representation of interactions between resin particles and L-Cyst molecules: **a** SH … π interaction, **b** NH … π interaction, **c** OH … π interaction, **d** CH … π interaction, **e** OH … N hydrogen bonding, **f** OH … O hydrogen bonding, **g** OH … S hydrogen bonding, **h** SH … O hydrogen bonding, **i** NH … O hydrogen bonding, **j** CH … O hydrogen bonding, **k** CH … N hydrogen bonding, and **l** CH … S hydrogen bonding

for the membrane and easy flow channels for the counter ion transportation. Uniform distribution of functional groups/L-Cyst on the membrane surface and in the bulk of the membrane matrix bring about further dispersion of the ionic clusters (in the membrane matrix), thus reducing the distance between ionic clusters ($d_{cluster}$), reducing the distance between regions without ions ($d_{ion\text{-}free}$), and generally increasing the distance between fixed ionic groups ($d_{fixed\text{-}ion}$). These changes surely provide superior regions for the membrane and easy flow channels for the counter ion transportation [28]. Figure 11 shows a schematic representation of these distances.

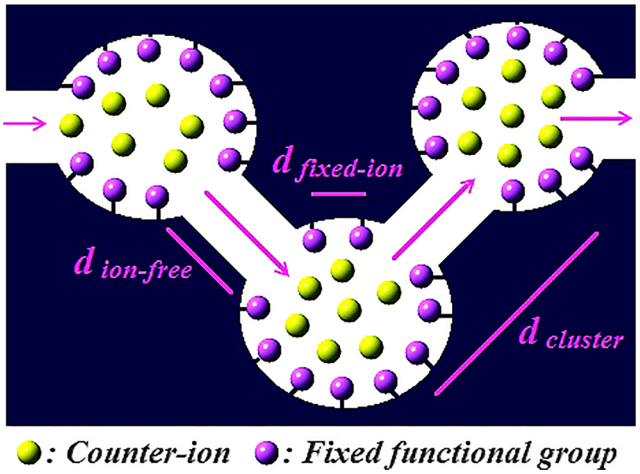

Fig. 11 Schematic cluster-network morphology of IEM with the average spacing between ionic clusters ($d_{cluster}$), between regions without ions ($d_{ion\text{-}free}$), and between fixed ionic groups ($d_{fixed\text{-}ion}$)

Figure 12 demonstrates the 3D images and Table 4 lists the data on the surface roughness of the resultant membranes. These parameters demonstrate that incorporation of L-Cyst causes the appearance of a smoother surface compared with that of the bare membrane. These alterations as a function of the L-Cyst quantity can be expressed by (i) filling of valleys on the membrane surface by the L-Cyst molecules and (ii) the existence of strong interactions between the resin and L-Cyst particles which prevent the agglomeration of L-Cyst in the membrane matrix. Generally, reduced roughness leads to (a) enhancement of antifouling characteristics during the separation process, (b) uniform distribution of boundary layer or flow over the surface, and (c) betterment of surface hydrophilicity of the membranes. Although membranes with higher surface roughness have higher surface area and, consequently, have more sites for interaction with H_2O molecules, steric hindrance prevents water molecules from transmission through their cavities. Therefore, these membranes generally have more contact angle values because, unlike membranes with a smoother surface, their surface cannot possess a systematically ordered network of hydrogen bonding between H_2O molecules.

Surface chemistry and surface structure are two determining factors for the water contact angle of IEMs. So, we expect IEMs which have surfaces with more hydrophilic functional groups and less roughness have less contact angle values. The membranes' surface hydrophilicity, which has a significant trace on ionic permeability, flux of ions, and antifouling

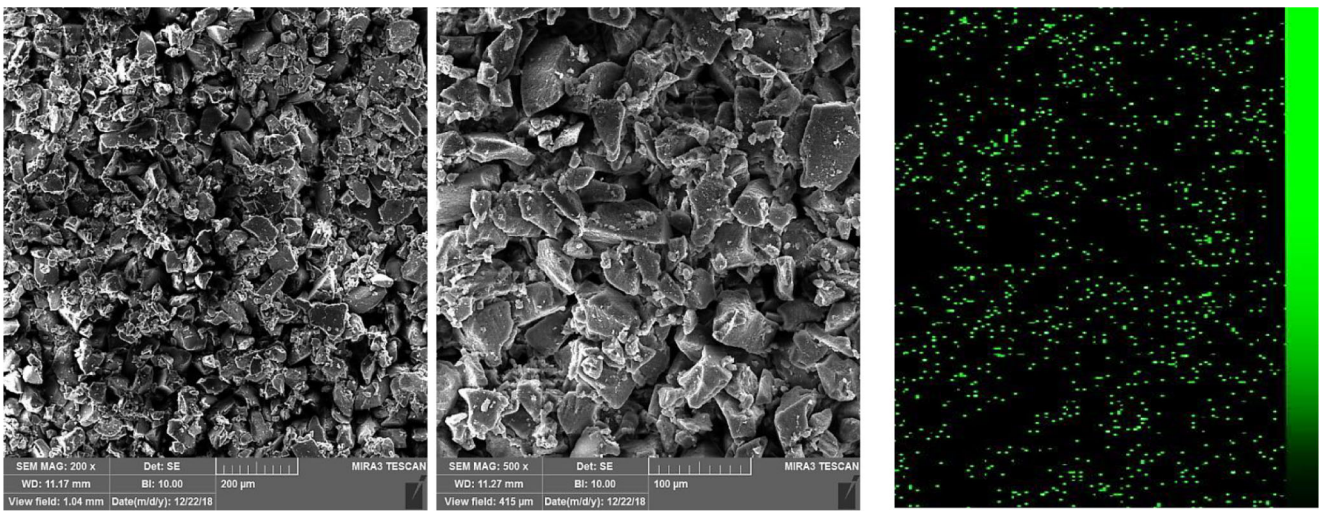

Fig. 10 Uniform distribution of particles (resin and L-Cyst); placement of L-Cyst molecules between resin particles: **a**, **b** SEM images and **c** EDX mapping of N

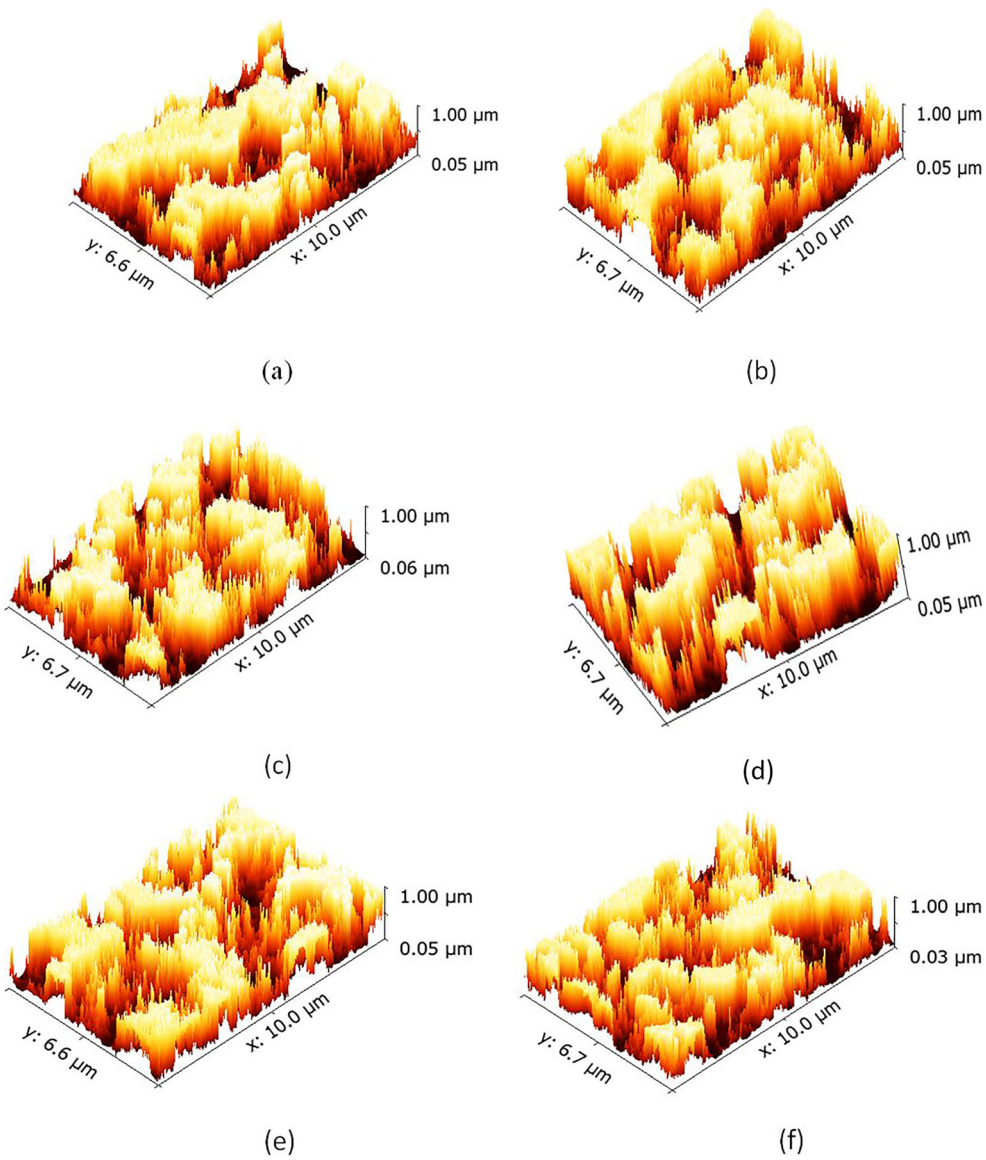

Fig. 12 3D images of prepared membranes with various ratios of L-Cyst: **a** 0.0 wt%, **b** 0.5 wt%, **c** 1.0 wt%, **d** 2.0 wt%, **e** 4.0 wt%, **f** 8.0 wt%

ability, was estimated by static water contact angle. Table 5 shows that modified membranes (S2 to S6) possess a lower contact angle, compared with the bare membrane (S1). The enhanced hydrophilicity of modified membranes was mostly accounted for the hydrophilicity of L-Cyst coming from its three functional groups (–SH, $–NH_2$, –COOH). The existence of hydrophilic functional groups on the surface of modified membranes allowed water droplets to create H-bonding (OH … S, OH … N, OH … O, SH … O, NH … O, COOH … O) with the surface and expand easily. Also, these H-bonding

Table 4 Roughness parameters for the prepared membranes with various ratios of L-Cyst

Membrane	Roughness average (nm)
Sample 1 (0.0 wt% L-Cyst)	103
Sample 2 (0.5 wt% L-Cyst)	69
Sample 3 (1.0 wt% L-Cyst)	66
Sample 4 (2.0 wt% L-Cyst)	61
Sample 5 (4.0 wt% L-Cyst)	58
Sample 6 (8.0 wt% L-Cyst)	56

Table 5 The effect of L-Cyst concentration on membrane water contact angle

Membrane	Contact angle (°)
Sample 1 (0.0 wt% L-Cyst)	112
Sample 2 (0.5 wt% L-Cyst)	84
Sample 3 (1.0 wt% L-Cyst)	80
Sample 4 (2.0 wt% L-Cyst)	72
Sample 5 (4.0 wt% L-Cyst)	68
Sample 6 (8.0 wt% L-Cyst)	63

interactions between surface and water molecules, which creates a water layer on the membrane surface, prevent adhesion of fouling agents. The fouling is able to increase the electric resistance of the membrane, decrease the ionic permeability and flux, and partly grow less the selectivity of the IEMs, which ended up having a higher power consumption and lower separation quality than those of the original state [29].

Water uptake and electrochemical properties

Equilibrium WU capacity is a determining parameter of IEMs, which has a considerable effect on their electrochemical properties. Generally, IEMs with a proper WU have better control on their transfer channels, and as a consequence, they show better selectivity. Additionally, excessively high WU may lead to poor dimensional stability, poor selectivity, and mechanical deterioration for these membranes. These realities underscore the significance of the WU parameter in membrane performance. Water in IEMs can exist in several states varying in binding energy with the membrane matrix. The concept in which water is divided into free and bound water is quite widely utilized. The bound water is subdivided into (i) hydration water which inters into the hydration shells of ion–dipole association, formed by a fixed functional ion exchange group and a counter ion; and (ii) confined water which is immobilized or confined in microporous channels where the electric double layers (EDLs) at the opposite pore walls overlap. The amount of free or bulk water, located outside ion–dipole associates, depends on the matrix's structure. The physicochemical features of bound water strongly differ from those of free water. Notably, freezing and melting of water in nanometer-sized pores happens at much lower temperatures than in the bulk water. Also, bound water has more spatial and orientation order in comparison to bulk water [12, 30, 31]. It is clear from the results (see Fig. 13) that the WU of all modified samples was higher than that of the bare one. This change in the WU capacity of modified membranes can be explained by the presence of three polar groups (–SH, $–NH_2$, –COOH) in L-Cyst molecules which impart the hydrophilicity of the membranes and then enhance the water adsorption in the membrane (increasing the bound water). Also, an increase of the membrane heterogeneity by using L-Cyst provides more free spaces for accommodating water molecules (increasing the free water). Also a declining trend was found for the membrane WU by increasing the L-Cyst concentration from 1 to 8 wt%. It appears that the higher compact structure of these samples is responsible for this event. Meanwhile, all the prepared membranes attained sufficient structural stabilities as confirmed by their negligible swelling (less than 5%).

Ionic permeability and flux are significant criteria for the membrane desalination process. A high flux membrane is highly favorable not only for reducing the membrane area but also for the increasing productivity. Electromigration, convection, diffusion, and surface site hopping are the four feasible mechanisms for the transportation of ions in the IEM matrix. Electromigration, convection, and diffusion occur mainly in the interstitial phase of free water, while surface site hopping of counter ions happens along the fixed ionic groups at the interface. The accurate transportation mechanisms of ions in an IEM are complicated and occur next to each other. Nevertheless, in ED systems (with the electric potential as the driving force), compared to electromigration, the contribution of diffusion and convection is small. Also, the surface site hopping occurs in the unclear degree of contribution [32]. The results (see Fig. 14) illustrate that compared to the bare membrane, all modified membranes had higher ionic permeability and flux. The plausible explanations for this event are as follows: (i) adsorptive characteristics of L-Cyst: L-Cyst comprises three negatively hydrophilic polar functional groups which impart adsorptive ability to the membrane; (ii) hydrophilicity of L-Cyst: the change in hydrophilicity of the membrane in the presence of L-Cyst has two effects: (a) ameliorating the ion transport between the solution and the membrane phase and (b) decreasing the fouling rates; the hydrophilic membrane surface has the potentiality to attract water molecules to make the hydrated layer, which acts as a buffer facing to the foulants; and (iii) more distribution of ionic clusters:

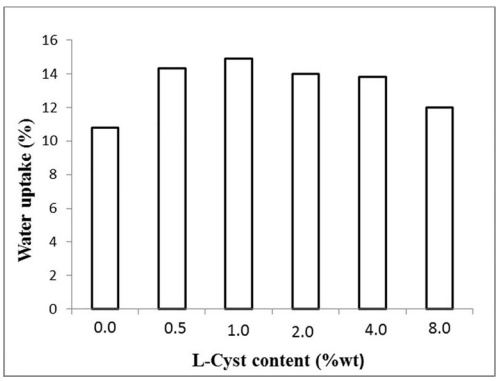

Fig. 13 The effect of L-Cyst concentration on water uptake

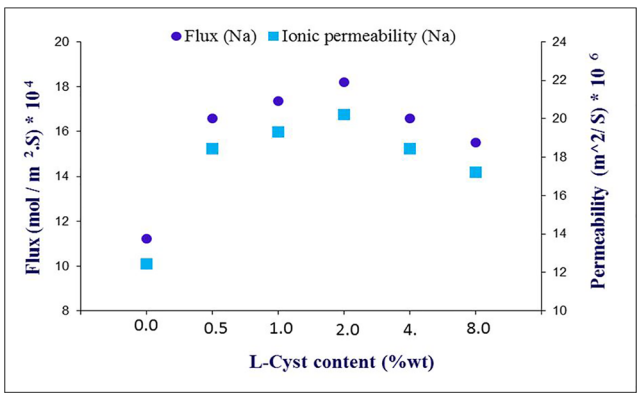

Fig. 14 Ionic permeability and flux of mixed matrix cation exchange membranes with various L-cysteine concentrations in NaCl ionic solution

better dispersion of ionic clusters brings about establishment of more ionic conducting channels which supply more sufficient number of continuous ion pathways through the membrane. This is because of the presence of the inert part which has no charge, no functional sites, and gaps or voids, located between the ionic clusters, restricts the transportation of ions. Furthermore, the distance between the solution bulk and membrane surface reduced thanks to the existence of –SH, $–NH_2$ and –COOH as polar groups on modified membranes' surfaces. Also, the results show that the ionic permeability and flux of modified samples were decreased by increasing the concentration of L-Cyst from 2 to 8 wt% in the membrane matrix. It is worth noting that these values are still higher than those of the unmodified sample. This reduction may be related to the formation of narrow ionic transfer channels in the membrane matrix by the L-Cyst, which impedes the transportation of ions through the membrane and declines the ion permeability and flux (this event was in agreement with WU results).

Membrane selectivity, the most essential feature in IEMs, makes the ED process efficient. Increased membrane selectivity will have a substantial role in the betterment of water quality and deletion of the requirement for additional separation stage. Figure 15 ((I) and (II)) demonstrates data pertaining to the membrane potential, transport number, and permselectivity of resultant membranes. These parameters had an increasing trend in all modified membranes in comparison to the bare one. The acceptable explanations for this event are as follows: (I) enhanced membrane WU promotes the dissociation of counter ions and fixed functional groups. Generally, counter ions can exist either as a solvated pair with the fixed ion group (Na^+ and R-SO_3^-), or in a condensed salt form ($NaSO_3$-R). While the membrane is partially hydrated with low WU, the counter ion strongly bonds with –SO_3^- functional groups and there are mostly ion pairs in the membrane (condensed salt form). This phenomenon leads to deactivating exchanger functional sites. As the WU increases, the water molecules promote the dissociation of counter ion and –SO_3^- functional group (solvated pair) [33]. (II) The specific structure of L-Cyst molecules increases their compatibility with the membrane body and then leads to their placement between the resin particles. It occurs because of the existence of strong interactions between them (as discussed earlier). Strong interactions followed by better distribution of particles make more dispersion of ionic clusters in nanocomposite IEMs (reducing the $d_{cluster}$, reducing the $d_{ion\text{-}free}$, and generally, increasing $d_{fixed\text{-}ion}$). The empowered dispersion of ionic clusters brings about (i) reduction of the interfacial gap and narrowing of the ionic channels (ionic clusters and interconnected channels) in the membrane and (ii) more dissociation of –SO_3H functional groups of resin particles. The $d_{fixed\text{-}ion}$ affects –SO_3H functional groups' dissociation ability in the resin. The inadequate large $d_{fixed\text{-}ion}$ makes the dissociation of these functional groups to be incomplete as a result of Coulombic repulsion of closely spaced negative charges confined to the polymer backbone. L-Cyst and resin particles' interaction resulted in the improvement of the $d_{fixed\text{-}ion}$. This change ensures higher exposure of –SO_3H functional groups needed for ion exchange and selective transportation of ions through the ionic channels of the modified membranes. Also, membranes with better distribution of clusters have smaller conducting channels which ultimately are thoroughly covered by the electric potential of their charged side walls. As a result, these channels show more ion selectivity. It is also possible that the EDLs formed on both sides of the pore wall overlap which provide highly selective transport of counter ions. Furthermore, irregular distribution of clusters impedes ion motion in a way that ions need to hop across ion-free regions in the channels to pass from one cluster to the next. This

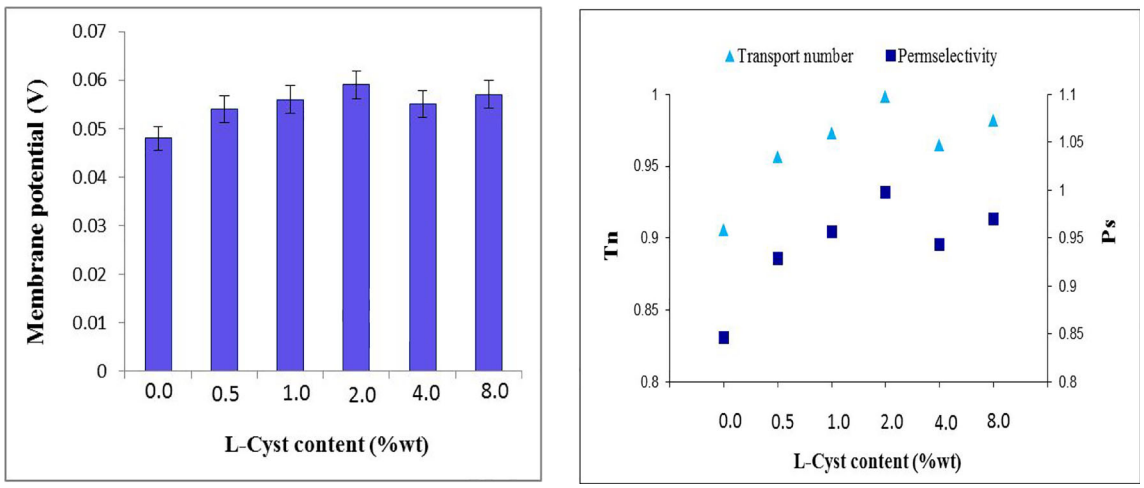

(I) (II)

Fig. 15 (I) Membrane potential. (II) Permselectivity and transport number of the prepared cation exchange membrane with various ratios of L-Cyst loading ratio in NaCl ionic solution

causes counter ion condensation in the clusters to increase and, subsequently, the Debye screening length (DSL) of the EDL to decrease which makes the dominance of channels in their transportation to be decreased. The thickness of the double layer decreases with electrolyte concentration increment due to charge shielding at the solid–solution interface. Further distribution of the ionic clusters and then the reduction of $d_{ion\text{-}free}$ prevent the accumulation of counter ions in the clusters and subsequently increase the DSL [28, 34]. In addition to providing more distribution of clusters, the specific structure of L-Cyst directly affected the improvement of the potential, transport number, and permselectivity of the modified membranes. This is because of (i) the existence of –COOH in L-Cyst which provides more cation exchange functional sites and (ii) the presence of a partial negative charge of its three functional groups (–SH, $–NH_2$, –COOH), which originates from their lone pair of electrons. All these bring about hindrance to the transport of co-ions across the membrane. Also, elemental mapping of Na^+ ions (see Fig. 16) can be taken as supplementary indication of (i) the presence of more cation exchange functional groups and (ii) more distribution of ionic clusters in the membrane matrix of modified membranes. Furthermore, a declining trend was found for the modified membranes by increasing of L-Cyst concentration from 2.0 to 4.0 wt%. Resin particle isolation by L-Cyst is a probable cause of this event (It is worth noting that these values are still higher than those of the membrane without L-Cyst loading). These parameters all increased again by increasing the L-Cyst concentration from 4 to 8 wt%. This is due to (i) the enhanced presence of L-Cyst in the membrane which provides more polar sites and (ii) the filling phenomenon of ion pathways which narrows down the channels and creates a compact structure.

Ionic conductivity and electrical resistance measurement are important tools to evaluate the ability of IEMs to conduct ions in the ED process. Table 6 lists the MER and IC of the optimum membranes (S3 and S4) as well as those of the bare one. Among them, the bare membrane MER and IC were 0.77 and 5, respectively, and incorporating the L-Cyst resulted in reduced MER values and increased IC values for the modified membranes. The acceptable explanations for this event are as follows: (I) the adsorption characteristics of L-Cyst opens up

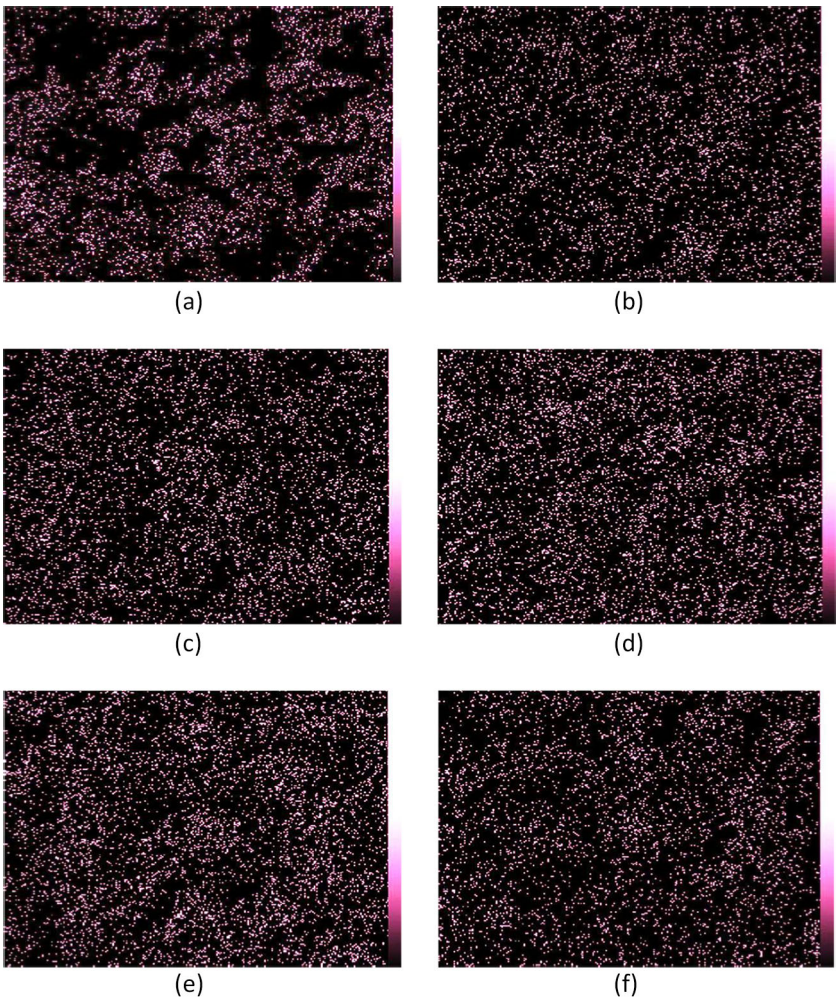

Fig. 16 EDX mapping of Na^+ element of prepared membranes with various ratios of L-cysteine content: **a** 0.0 wt%, **b** 0.5 wt%, **c** 1.0 wt%, **d** 2.0 wt%, **e** 4.0 wt%, **f** 8.0 wt%

Table 6 MER and IC of the prepared membranes

Membrane	MER (Ω)	IC (S/cm) × 10^4
Sample 1 (0.0 wt% L-Cyst)	0.77	5
Sample 3 (1.0 wt% L-Cyst)	0.51	7.5
Sample 4 (8.0 wt% L-Cyst)	0.29	13.3

the facilities of ion transport between the solution and membrane phase and, subsequently, the cation immigration across the membrane. In fact, the presence of three polar groups (–SH, $–NH_2$, –COOH) improved the interactions between ions and L-Cyst. Also, the membrane surface active sites were enhanced, thanks to their improved surface hydrophilicity. (II) Homogeneously distributed ionic clusters promote the transport of the ions through the additional shorter conducting channels. Membranes with homogeneously distributed ionic clusters have more interconnected channels and shorter pathways of ions across themselves. As a matter of fact, the hydrophobic polymer matrix is virtually impermeable for ions so that their transportation is only possible via conducting channels. Thus, the lack of uniform distribution of these channels brings about much longer pathways to the other side of the membrane, which consequently increases the MER. (III) Enhanced membrane WU improves the mobility of ions through conducting channels. While the membrane is partially hydrated with low WU, the counter ions strongly bond with $–SO_3^-$ functional groups and there are mostly ion pairs in the matrix. As the WU increases, the water molecules promote the dissociation of counter ions and fixed functional groups and yield more free ions in the matrix, thereby increasing the conductivity of the membranes. The above discussion elucidates that the conductivity of IEMs is strongly tied to the interactions between functional groups, counter ions, and water molecules in the membrane matrix.

The electrodialysis experiment was also utilized to study the ability of the modified membranes in Pb^{2+} ion removal from wastewater. The dialytic rate, CE, and energy consumption (*E*) for the prepared membranes (sample 1—unmodified membrane and sample 4 and sample 6—modified membranes) were investigated. The obtained results (Fig. 17) demonstrate that utilizing L-Cyst in the membrane matrix leads to a decrease of *E*, an increase of CE, and dialytic rate for Pb^{2+} ion separation from the solution. This corroborates that modified samples have a high capacity for Pb^{2+} ion removal from water. The results show that the removal of Pb^{2+} ions decreased over

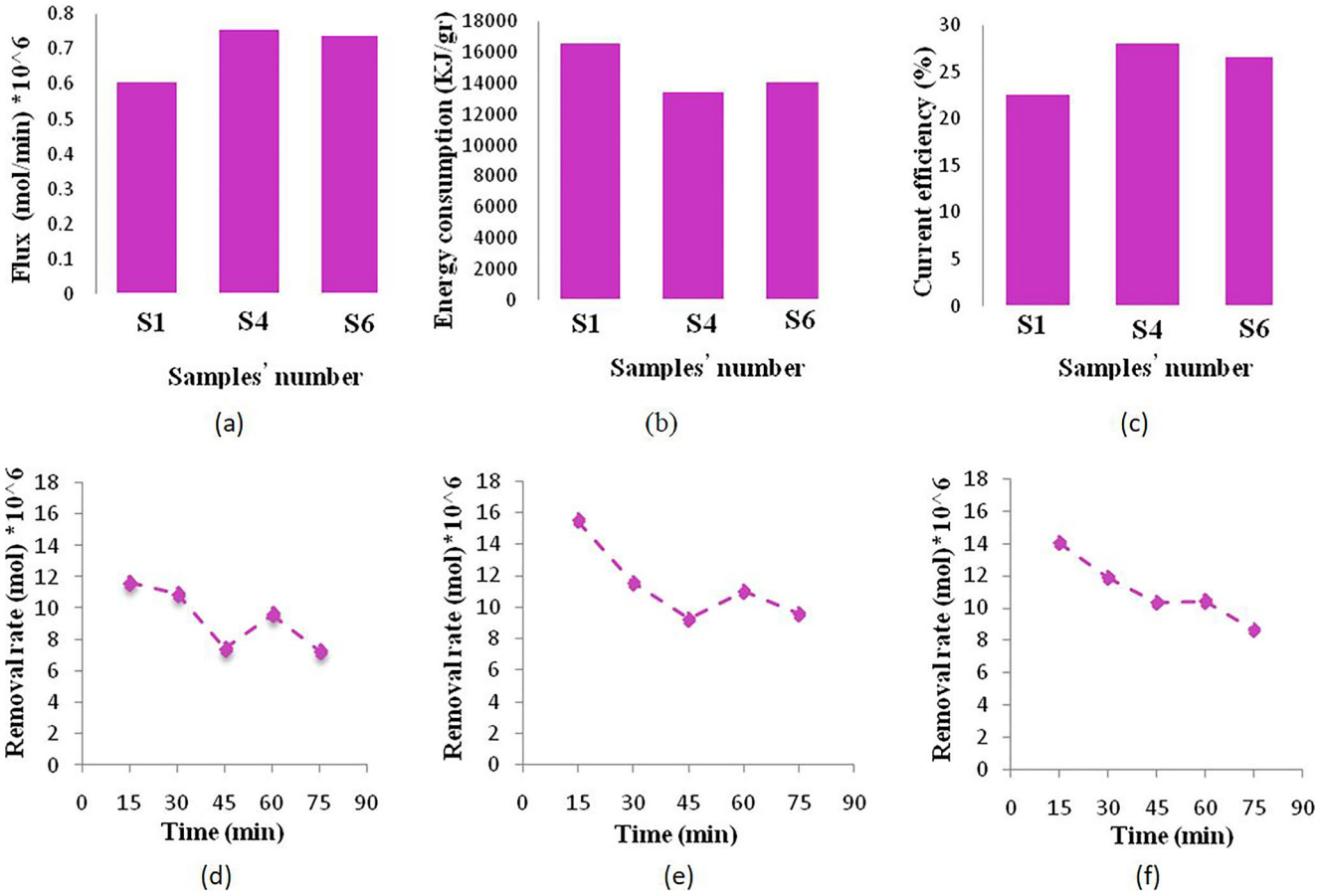

Fig. 17 **a** Flux. **b** Energy consumption. **c** Current efficiency. **d**–**f** Lead removal rate at applied potential. S1 (unmodified membrane), S4 and S6 (modified membranes)

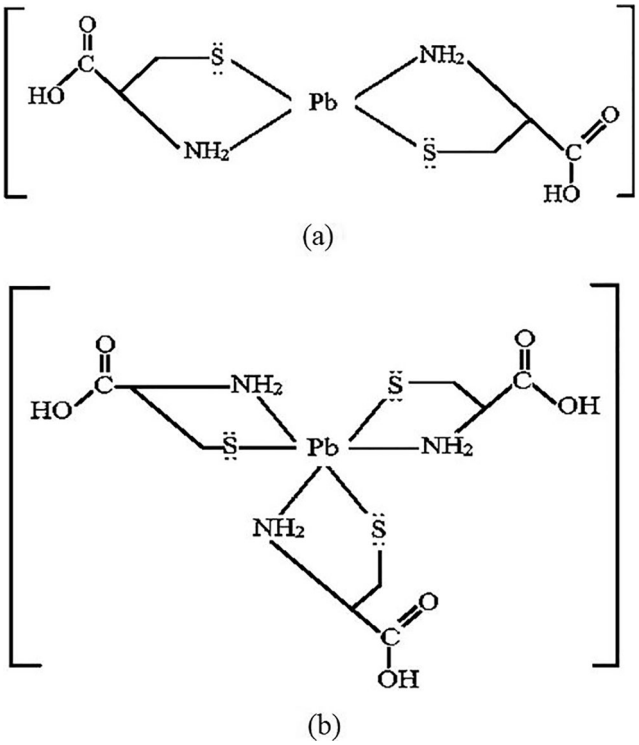

Fig. 18 The most possible binding mechanisms of Pb^{2+} ion onto L-Cyst molecule

time. This is due to occupying adsorption sites over time. The enhancement of dialytic rate for Pb^{2+} ion separation from the solution can be linked to the specific structure of L-Cyst, which provided more adsorption sites and surface hydrophilicity for the modified sample. The main adsorption sites for Pb^{2+} ions are thiol (–SH), amine ($–NH_2$), and carboxyl (–COOH) in L-Cyst. The lone pair electrons in these functional groups are well reciprocated by the vacant orbitals of Pb^{2+} ions. The most possible binding mechanisms of Pb^{2+} ion onto L-Cyst molecule are demonstrated in Fig. 18. Also, Fig. 19 represents the EDX spectrum and elemental mapping analysis of the membrane surface after the Pb^{2+} ion removal study. This analysis confirms the interaction of Pb^{2+} ions with the active surface of the membrane.

In this study, to investigate the reproducibility of the performance of fabricated membranes, the membranes used were taken from the cell and washed by an ultrasonic cleaner and kept in DI water for 5 h. Consequently, the ability of the regenerated membranes in terms of Pb^{2+} ion removal was estimated and compared with the performance of the membranes used. The obtained data indicated a slight decrease of the performance for sample 4 and a slight increase for sample 6 (see Fig. 20). The slight decrease in flux for sample 4 (less than 5%) shows the potential and strong adsorptive affinity of L-Cyst toward Pb^{2+} ion attraction which makes difficult the release of these ions. Also, the plausible explanation for the increasing flux in sample 6 is that in this sample (containing 8.0 wt% L-Cyst) Pb^{2+} ions form a complex with three L-Cyst molecules during adsorption due to its having more L-Cyst on its structure. This kind of complex has a negative charge that causes adsorption to be kept (see Fig. 18b).

Another point to note is that sample 4 (containing 2.0 wt% L-Cyst) showed both high ionic selectivity and high ionic permeability. The balance between high selectivity and high permeability of ions observed in this sample could be resulted from the transport scenario demonstrated in Fig. 21 (II). Generally, the size of the transport channels has a drastic affiliation on selectivity and permeability of IEMs. Fabrication of membranes with both high selectivity and high permeability has been a long-standing challenge in membrane science which can be solved with controlling the size of the pores and providing a large number of uniformly sized pores. This approach leads to prevail the trade-off relation between the ionic permeability and selectivity. As represented in Fig. 21, membranes containing small pore size which their

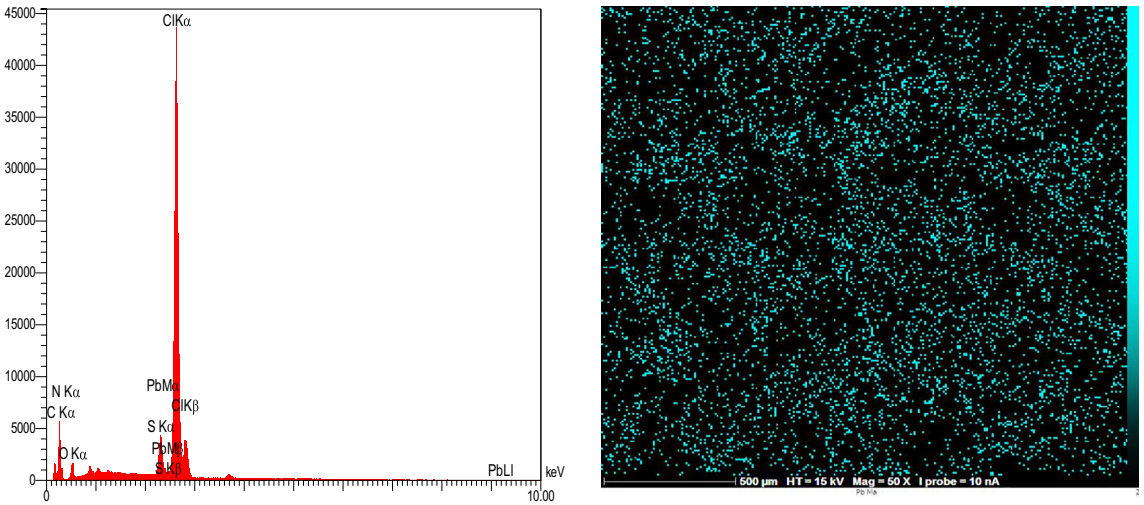

Fig. 19 The EDX spectrum and elemental mapping analysis of the membrane surface after Pb^{2+} ion removal study

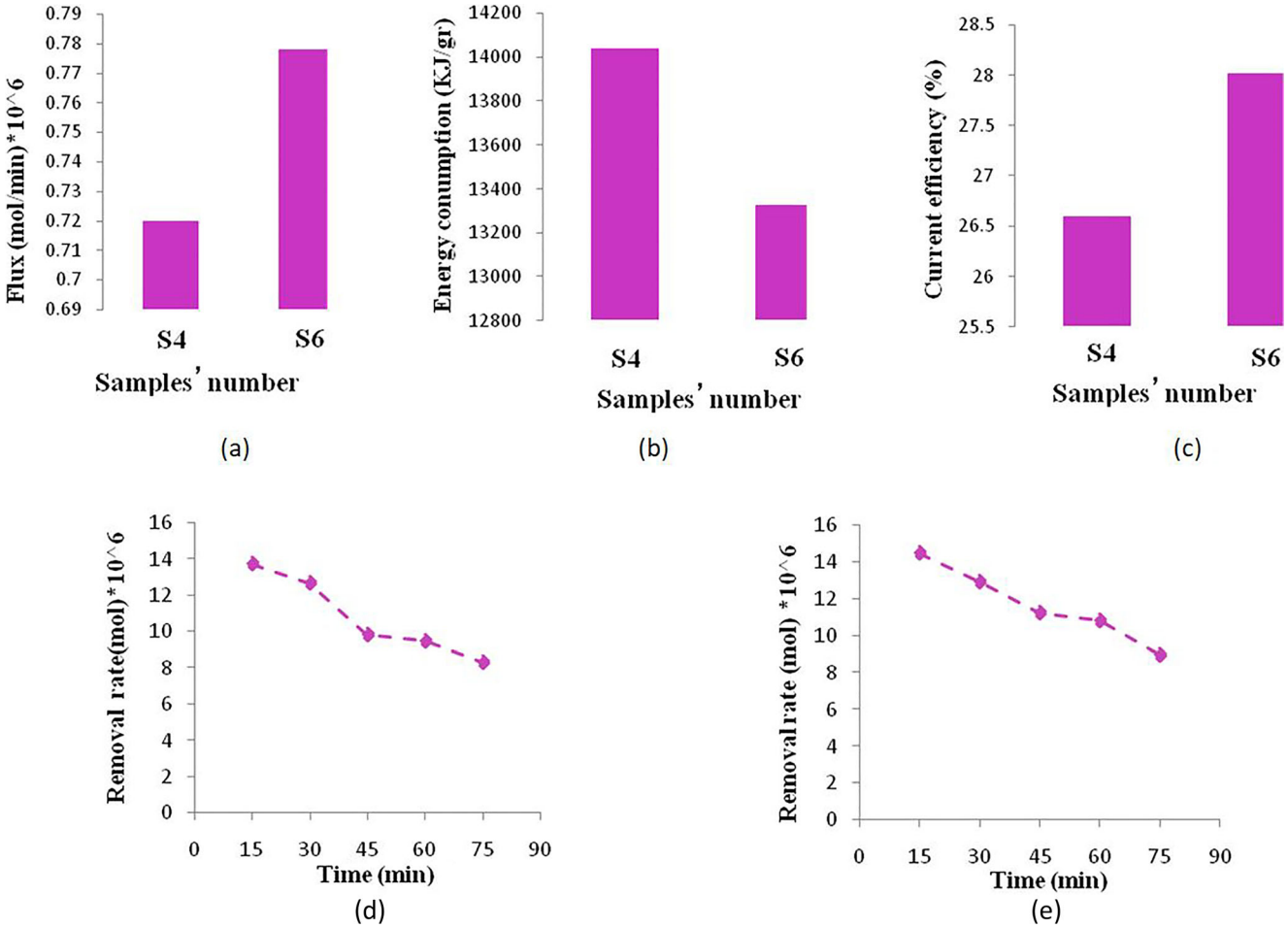

Fig. 20 **a** Flux. **b** Energy consumption. **c** Current efficiency. **d**, **e** Lead removal rate at applied potential after regeneration. S4 and S6 (modified membranes)

pore size is smaller than the hydration radius of the ions often show high selectivity but low permeability of ions since dehydration becomes dominant (Fig. 21 (I)). On the other hand, membranes containing large pore size which their pore size is much larger than the DSL of the EDL often show high permeability of ions but nearly no selectivity (Fig. 21 (III)). Since the electric potential of their charged side walls cannot cover the whole channel. And finally when the pore size of IEMs is between the two cases, the IEM shows a balance between selectivity and permeability together (Fig. 21 (II)) [35].

The final point to note is that the properties of the modified membranes in this study are comparable with those of commercial HCEMs and other reported ones (see Tables 7 and 8).

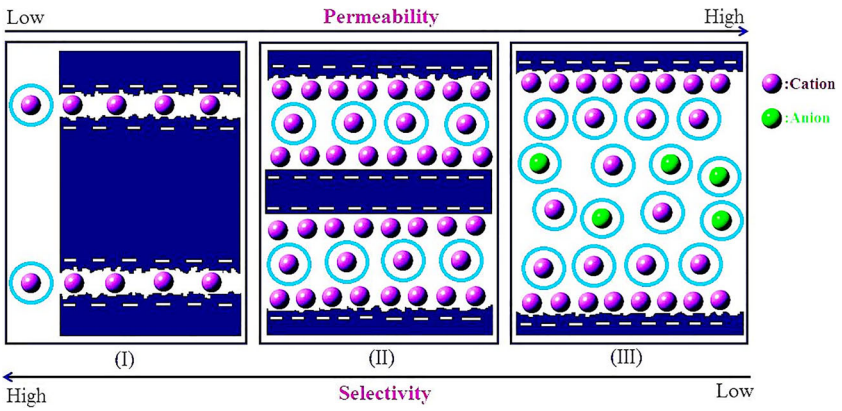

Fig. 21 Schematic representation of three ionic transport mechanisms as the pore size increases in CEMs

Table 7 Comparison between the electrochemical properties of the prepared membrane in this study and some commercial membranes [36–38]

Membrane	Permselectivity[a] (%)	Electrical resistance[b] (Ω cm^2)
Unmodified membrane (S1) (HCEM)[c]	> 84	15
Modified membrane (S4) (HCEM)	> 99	5.6
Ralex® CMH-PES (HCEM)	> 92	< 10.0
Ionics Inc., USA, CR61-CMP (HCEM)	_	11
CSMCRI, India (HCEM)	87	4.0–6.0
Ionics Inc., USA (61CZL386) (HCEM)	_	9
RAI Research Corp., USA R-5010-H	95	8–12
Tokuyama Soda Co. Ltd., Japan (Neosepta CMX)	97	1.8–3.8
FuMA-Tech GmbH, Germany FKB	–	5–10
Fumasep® FKD	> 95	< 3

[a] Measured in 0.1/0.01 M NaCl solution

[b] Measured in 0.5 M NaCl solution

[c] Heterogeneous cation exchange membrane

Conclusion

The MEP of the L-Cyst molecule and resin particle showed that both particles have appropriate reactive sites for electrophilic and nucleophilic attack. Furthermore, the interaction energy between L-Cyst molecule and resin particle was calculated which confirmed the presence of strong interactions between them. Elemental mapping, SEM, and SOM images of the resultant membranes represented a relatively uniform surface and particle distribution. Membrane water uptake and surface hydrophilicity were enhanced in the presence of L-Cyst. The modified membranes showed better selectivity, electrical conductivity, and ionic permeability compared to the bare one. The modified membranes demonstrated better selectivity (up to 99%), lower electrical resistance (up to ~ 5–6 Ω cm^2), and better ionic permeability compared to the bare one (in NaCl ionic solution). Also, utilizing membranes on the removal of Pb^{2+} ions showed that the superior membrane (containing 2.0 wt% L-Cyst) had lower energy consumption, more dialytic rate, and current efficiency compared to the unmodified sample.

Table 8 Comparison of the performance characteristics of modified IEM reported in this paper with those reported by earlier studies [19, 20, 39–41]

Membrane	Permselectivity (%)	Electrical resistance (Ω cm^2)
Modified membrane (S4) (HCEM)[a]	> 99	5.6
HCEM (4.0 wt%–GO Ns) [20]	> 89	6.5–7
HCEM (2.0 wt%–zeolite NPs) [39]	> 88	6–7
HCEM (4.0 wt%–ZnQ_2 NPs) [19]	> 98	8–9
HCEM (8.0 wt%–Al_2O_3 NPs) [40]	> 80	6–7
HCEM (0.5 wt%–Fe_3O_4/PAA NPs) [41]	> 84	11–12

[a] Heterogeneous cation exchange membrane

Funding information The authors gratefully acknowledge Arak University for the financial support during this research.

References

1. Zhang DY, Hao Q, Liu J, Shi YS, Zhu J, Su L, Wang Y (2018) Antifouling polyimide membrane with grafted silver nanoparticles and zwitterion, separation and purification technology. Sep Purif Technol 192:230–239
2. Xu GR, Xu JM, Su HC, Liu XY, Li L, Zhao HL, Feng HJ, Das R (2019) Two-dimensional (2D) nanoporous membranes with sub-nanoporous in reverse osmosis desalination: latest developments and future directions. Desalination 451:18–34
3. Luo F, Wang Y, Jiang C, Wu B, Feng H, Xu T (2017) A power free electrodialysis (PFED) for desalination. Desalination 404:138–146
4. Mondal AN, Zheng C, Cheng C, Miao J, Hossain MM, Emmanuel K, Khan MI, Afsar NU, Ge L, Wu L, Xu T (2016) Novel silica-functionalized aminoisophthalic acid-based membranes for base recovery via diffusion dialysis. J Membr Sci 507:90–98
5. Babilas D, Dydo P (2018) Selective zinc recovery from electroplating wastewaters by electrodialysis enhanced with complex formation. Sep Purif Technol 192:419–428
6. Malek P, Ortiz JM, Herbruggen HMAS (2016) Decentralized desalination of brackish water using an electrodialysis system directly powered by wind energy. Desalination 377:54–64
7. Han L, Galier S, Balmann HR (2016) Transfer of neutral organic solutes during desalination by electrodialysis: influence of the salt composition. J Membr Sci 511:207–218
8. Bakangura E, Wu L, Ge L, Yang Z, Xu T (2016) Mixed matrix proton exchange membranes for fuel cells: state of the art and perspectives. Prog Polym Sci 57:103–152
9. Ran J, Wu L, He Y, Yang Z, Wang Y, Jiang C, Ge L, Bakangura E, Xu T (2017) Ion exchange membranes: new developments and applications. J Membr Sci 522:267–291
10. Vogel C, Haack JM (2014) Preparation of ion-exchange materials and membranes. Desalination 342:156–174
11. Yee RSL, Rozendal RA, Zhang K, Ladewig BP (2012) Cost effective cation exchange membranes: a review. Chem Eng Res Des 90: 950–959
12. Kononenko N, Nikonenko V, Grande D, Larchet C, Dammak L, Fomenko M, Volfkovich Y (2017) Porous structure of ion exchange membranes investigated by various techniques. Adv Colloid Interf Sci 246:196–216
13. Bagbi Y, Sarswat A, Mohan D, Pandey A, Solanki PR (2017) Lead and chromium adsorption from water using L-cysteine functionalized magnetite (Fe_3O_4) nanoparticles. Sci Rep 7
14. Javan MB, Soltani A, Lemeski ET, Ahmadi A, Moazen Rad S (2016) Interaction of $B_{12}N_{12}$ nano-cage with cysteine through various functionalities: a DFT study. Superlattice Microst 100:24–37
15. Efome JE, Rana D, Matsuura T, Lan CQ (2018) Experiment and modeling for flux and permeate concentration of heavy metal ion in adsorptive membrane filtration using a metal-organic framework incorporated nanofibrous membrane. Chem Eng J 352:737–744

16. Efome JE, Rana D, Matsuura T, Lan CQ (2019) Effects of operating parameters and coexisting ions on the efficiency of heavy metal ions removal by nano-fibrous metal-organic framework membrane filtration process. Sci Total Environ 674:355–362
17. Efome JE, Rana D, Matsuura T, Lan CQ (2018) Insight studies on metal-organic framework nanofiltration membrane adsorption and activation for heavy metal ions removal from aqueous solution. ACS Appl Mater Interfaces 10:18619–18629
18. Efome JE, Rana D, Matsuura T, Lan CQ (2018) Metal-organic frameworks supported on nanofibers to remove heavy metals. J Mater Chem A 6:4550–4555
19. Hosseini SM, Jashni E, Jafari MR, Van der Bruggen B, Shahedi Z (2018) Nanocomposite polyvinyl chloride-based heterogeneous cation exchange membrane prepared by synthesized ZnQ_2 nanoparticles: ionic behavior and morphological characterization. J Membr Sci 560:1–10
20. Hosseini SM, Jashni E, Habibi M, Nemati M, Van der Bruggen B (2017) Evaluating the ion transport characteristics of novel graphene oxide nanoplates entrapped mixed matrix cation exchange membranes in water deionization. J Membr Sci 541:641–652
21. Hosseini SM, Jashni E, Habibi M, Van der Bruggen B (2018) Fabrication of novel electrodialysis heterogeneous ion exchange membranes by incorporating PANI/GO functionalized composite nanoplates. Ionics 24:1789–1801
22. Hosseini SM, Jashni E, Amani S, Van der Bruggen B (2017) Tailoring the electrochemical properties of ED ion exchange membranes based on the synergism of TiO_2 nanoparticles-co-GO nanoplates. J Colloid Interface Sci 505:763–775
23. Hosseini SM, Madaeni SS, Khodabakhshi AR, Zendehnam A (2010) Preparation and surface modification of PVC/SBR heterogeneous cation exchange membrane with silver nanoparticles by plasma treatment. J Membr Sci 365:438–446
24. Hosseini SM, Madaeni SS, Khodabakhshi AR (2010) Preparation and characterization of PC/SBR heterogeneous cation exchange membrane filled with carbon nano-tubes. J Membr Sci 362:550–559
25. Hosseini SM, Madaeni SS, Khodabakhshi AR (2010) Preparation and characterization of ABS/HIPS heterogeneous cation exchange membranes with various blend ratios of polymer binder. J Membr Sci 351:178–188
26. Huang SW, Lin YF, Li YX, Hu C-C, Chiu T-C (2019) Synthesis of fluorescent carbon dots as selective and sensitive probes for cupric ions and cell imaging. Molecules 24:1785
27. Dzade NY, Roldan A, Leeuw NH (2016) Surface and shape modification of mackinawite (FeS) nanocrystals by cysteine adsorption: a first-principles DFT-D2 study. Phys Chem Chem Phys 18:32007–32020
28. Lwoya BS, Albert JNL (2015) Nanostructured block copolymers for proton exchange membrane fuel cells. Energy and Environmental Focus 4:278–290
29. Suwal S, Doyen A, Bazinet L (2015) Characterization of protein, peptide and amino acid fouling on ion-exchange and filtration membranes: review of current and recently developed methods. J Membr Sci 496:267–283
30. Kittaka S, Ishimaru S, Kuranishi M, Matsuda T, Yamaguchi T (2006) Enthalpy and interfacial free energy changes of water capillary condensed in mesoporous silica, MCM-41 and SBA-15. Phys Chem Chem Phys 8:3223–3231
31. Morishige K, Iwasaki H (2003) X-ray study of freezing and melting of water confined within SBA-15. Langmuir 19:2808–2811
32. Luo T, Abdu S, Wessling M (2018) Selectivity of ion exchange membranes: a review. J Membr Sci 555:429–454
33. Cassady HJ, Cimino EC, Kumar M, Hickner MA (2016) Specific ion effects on the permselectivity of sulfonated poly (ether sulfone) cation exchange membranes. J Membr Sci 508:146–152
34. A Alabi, A Alhajaj, L Cseri, G Szekely, P Budd, L Zou (2018) Review of nanomaterials-assisted ion exchange membranes for electromembrane desalination. NPJ Clean Water 10
35. R Wang, M Wang, F Liu, S Ding, X Wang, G Du, J Liu, P Apel, P Kluth, Ch Trautmann, Y Wang, Ultrafast ion sieving using nanoporous polymeric membranes. Nature Communications 596(2018)
36. Nagarale RK, Gohil GS, Shahi VK (2006) Recent developments on ion-exchange membranes and electro-membrane processes. Adv Colloid Interf Sci 119:97–130
37. Dlugolecki P, Nymeijer K, Metz S, Wessling M (2008) Current status of ion exchange membranes for power generation from salinity gradients. J Membr Sci 319:214–222
38. Xu T (2005) Ion exchange membranes: state of their development and perspective. J Membr Sci 263:1–29
39. Hosseini SM, Rafiei S, Hamidi AR, Moghadassi AR, Madaeni SS (2014) Preparation and electrochemical characterization of mixed matrix heterogeneous cation exchange membranes filled with zeolite nanoparticles: ionic transport property in desalination. Desalination 351:138–144
40. Hosseini SM, Gholami A, Koranian P, Nemati M, Madaeni SS, Moghadassi AR (2014) Electrochemical characterization of mixed matrix heterogeneous cation exchange membrane modified by aluminum oxide nanoparticles: mono/bivalent ionic transportaion. J Taiwan Inst Chem Eng 45:1241–1248
41. Nemati M, Hosseini SM (2016) Fabrication and electrochemical property modification of mixed matrix heterogeneous cation exchange membranes filled with Fe_3O_4/PAA core-shell nanoparticles. Ionics 22:899–909